HHS Public Access

Author manuscript

Langmuir. Author manuscript; available in PMC 2016 July 27.

Published in final edited form as:

Langmuir. 2015 November 17; 31(45): 12339–12347. doi:10.1021/acs.langmuir.5b02902.

Biofunctionalization of Large Gold Nanorods Realizes Ultrahigh-Sensitivity Optical Imaging Agents

Elliott D. SoRelle[†,‡,§], **Orly Liba**[†,§,‖], **Zeshan Hussain**[†,§], **Milan Gambhir**[†,§], and **Adam de la Zerda**[†,‡,§,‖,*]

[†]Molecular Imaging Program at Stanford, Bio-X Program, Stanford University, Palo Alto, California 94305, United States

[‡]Biophysics Program, Stanford University, Palo Alto, California 94305, United States

[§]Departments of Structural Biology, Stanford University, Palo Alto, California 94305, United States

[‖]Electrical Engineering, Stanford University, Palo Alto, California 94305, United States

Abstract

Gold nanorods (GNRs, ~ 50 × 15 nm) have been used ubiquitously in biomedicine for their optical properties, and many methods of GNR biofunctionalization have been described. Recently, the synthesis of larger-than-usual GNRs (LGNRs, ~ 100 × 30 nm) has been demonstrated. However, LGNRs have not been biofunctionalized and therefore remain absent from biomedical literature to date. Here we report the successful biofunctionalization of LGNRs, which produces highly stable particles that exhibit a narrow spectral peak (FWHM ~100 nm). We further demonstrated that functionalized LGNRs can be used as highly sensitive scattering contrast agents by detecting individual LGNRs in clear liquids. Owing to their increased optical cross sections, we found that LGNRs exhibited up to 32-fold greater backscattering than conventional GNRs. We leveraged these enhanced optical properties to detect LGNRs in the vasculature of live tumor-bearing mice. With LGNR contrast enhancement, we were able to visualize tumor blood vessels at depths that were otherwise undetectable. We expect that the particles reported herein will enable immediate sensitivity improvements in a wide array of biomedical imaging and sensing techniques that rely on conventional GNRs.

Graphical Abstract

[*]**Corresponding Author**. adlzstanford.edu.

ASSOCIATED CONTENT

Supporting Information

The Supporting Information is available free of charge on the ACS Publications website at DOI: 10.1021/acs.langmuir.5b02902.

Detailed methods, statistics, and all original data from stability assays are presented in this section. Supporting figures, results, and discussion are also provided (PDF).

Author Contributions

The manuscript was written through contributions of all authors. All authors have given approval to the final version of the manuscript.

The authors declare no competing financial interest.

NOTE ADDED AFTER ASAP PUBLICATION

This paper was published on the Web on October 30, 2015 with incorrect layout on the second and third pages. The corrected version was reposted on November 3, 2015.

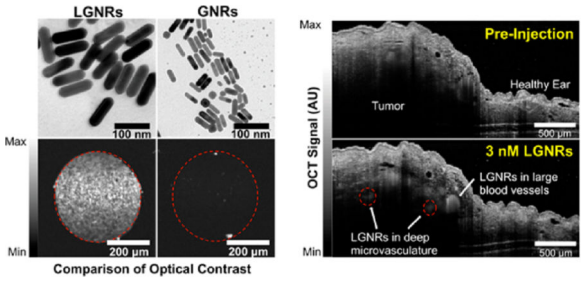

1. INTRODUCTION

Nanoparticles can be synthesized in a vast array of shapes and sizes to suit specific needs in biomedical therapy and imaging. Gold Nanorods (GNRs) have been particularly useful therapeutic[1–6] and imaging contrast agents[7–19] ever since protocols for simple GNR synthesis were first reported.[20–23] These original methods produced GNRs with approximate dimensions of 50 × 15 nm. Groups have adapted these GNRs for applications including photothermal therapy,[1,3,4] two-photon luminescence,[7–9] Surface-Enhanced Raman Scattering (SERS),[109–13] photoacoustic imaging,[149–17] and optical coherence tomography (OCT).[18,19] Recently, methods to produce significantly larger GNRs (up to 150 × 50 nm) have been developed.[24] Based on theoretical modeling,[259–28] these large GNRs (LGNRs) are predicted to offer advantages in numerous biomedical imaging techniques due to greater absorption and scattering cross sections relative to their commonly used smaller counterparts.

Despite their clear advantages, LGNRs have not been utilized in biomedical studies to date. The greatest barrier to employing LGNRs in biomedical studies is the need for robust surface chemistry to achieve particle stability, nontoxicity, and biofunctionality for targeted imaging and therapy. While numerous groups have stabilized GNRs by replacing residual cetyltrimethylammonium bromide (CTAB, left over from GNR synthesis) with thiolated polyethylene glycol (PEG-SH) reagents[3,29] or through polyelectrolyte overcoating,[1,4,7,10,30–32] no study to date has described surface modifications and biological use of LGNRs. Because of their significant size difference, it is unclear whether coating methods that work for GNRs will also work for LGNRs. From a practical standpoint, functional surface chemistry methods for coating LGNRs must exist to realize their advantages as biomedical imaging agents. Furthermore, particles must remain stable throughout (i) multiple washing steps to remove cytotoxic surfactants and (ii) conjugation reactions with biomolecules of interest.[30,31] Thus, a rigorous characterization of LGNR stability and surface chemistry must be explored if their optical superiority to conventional GNRs is to be leveraged.

To explore whether LGNRs can be successfully adapted for biological studies, we compared the stability of GNRs (~50 × 15 nm) and LGNRs (~100 × 30 nm) as a function of surface coating. We found that while conventional PEG surface coating stabilized GNRs, it did not stabilize LGNRs. We explored this difference in mechanistic detail and found that it arose from the nature of the surfactant-directed growth process. To circumvent the instability of LGNRs coated with PEG, we used poly(sodium 4-styrenesulfonate) (PSS) to render LGNRs

that exhibited excellent colloidal stability. Importantly, we also developed methods to further functionalize PSS-coated LGNRs with biological ligands of interest. Finally, we used OCT to demonstrate that LGNRs produce much stronger optical signals than GNRs and therefore enable vast improvements to imaging sensitivity both in vitro and in vivo.

2. EXPERIMENTAL SECTION

Particle Synthesis and Characterization

GNRs and LGNRs were synthesized at two different peak wavelengths each (I: ~ 750 nm and II: ~ 800 nm) using protocols described by El-Sayed[23] and Murray,[24] respectively. Particle morphologies and size distributions were characterized from transmission electron micrographs acquired with a JEOL TEM 1400. Absorbance measurements for each particle type were obtained using a Cary 6000i spectrometer operating in transmission mode from 400 to 1100 nm.

Size-Dependent Stability Characterization

(L)GNRs were prepared with one of three surface coatings: CTAB, mPEG-SH (MW ~ 5 kDa), or PSS (MW ~ 70 kDa), resulting in (L)GNRs-CTAB, (L)GNRs-mPEG, and (L)GNRs-PSS, respectively. Coated particles were then washed through multiple rounds of centrifugation at 2550*g* followed by resuspension in distilled deionized (DDI) water. Stability trends for (L)GNRs were characterized by changes in spectral bandwidth (a proxy for colloidal stability/particle aggregation) as a function of surface coating and the number of wash cycles. (L)GNR zeta potentials were also measured using electrophoretic light scattering (ELS) after each round of washing. Successful surface coating was verified through TEM, Vis-NIR spectrometry, and dynamic light scattering (DLS) characterization following particle incubation with PSS or various PEG-SH ligands. Extensive additional methods to investigate the mechanisms of size-dependent stability trends are provided and discussed in the Supporting Information (SI).

LGNR Biostability

The stability of LGNRs-PSS in biological environments was also assayed. LGNRs-mPEG and LGNRs-PSS were prepared as 1 mL aliquots and incubated with 500 μL Fetal Bovine Serum (FBS). As an additional test of LGNR biostability and potential toxicity, LGNRs-PSS-mPEG were prepared and injected at high doses (up to 80 mg/kg) into female nude (nu^-/nu^-) and C57BL/6 mice. Injected mice were monitored over a period of 3 months for signs of distress.

LGNR Functionalization for Specific Ligand–Receptor Binding

LGNRs-PSS were incubated with either mPEG-SH or Biotin-PEG-SH and washed 2× to remove excess reagents (resulting in LGNRs-PSS-mPEG and LGNRs-PSS-PEG-Biotin, respectively). LGNRs-PSS-PEG-Biotin and LGNRs-PSS-mPEG were further incubated with FBS to simulate biological environments and then mixed with streptavidin-coated polystyrene beads in water to assay binding specificity. These incubation conditions were repeated with streptavidin-coated beads that were prereacted with excess biotin to confirm the molecular specificity of the LGNR binding interaction.

Optical Comparison of GNRs vs LGNRs

GNRs and LGNRs were prepared to equal concentrations (2×10^{10} nps/mL) and (separately) to equal optical density (OD 1) in glass capillary tubes and scanned using a spectral domain optical coherence tomography (SD-OCT) probe. The OCT signal from each sample was quantified using region of interest analysis to determine the relative scattering intensity of GNRs and LGNRs (see Detailed Experimental Methods in SI). LGNRs were also prepared in water at various concentrations ranging from $2 \times 10^{8} – 2 \times 10^{10}$ nps/mL (500 fM to 50 pM) to determine imaging sensitivity for LGNR detection.

LGNR Contrast Enhancement in vivo

LGNRs-PSS-mPEG (250 μL of 23.5 nM, peak wavelength = 804 nm) were injected intravenously into a female nude mouse (anesthetized with 1% isoflurane inhalation) bearing a U87MG tumor xenograft in the right ear pinna. OCT images were acquired pre- and postinjection and compared to assess the presence of LGNR contrast-enhancement in healthy and tumor microvasculature.

3. RESULTS

Particle Morphology and Spectra

TEM images reveal the significant size differences between GNRs (~50 × 15 nm) and LGNRs (~100 × 30 nm) (Figure 1a and SI Figure S1). Interestingly, LGNRs exhibited greater monodispersity than GNRs as evidenced by particle size distributions (Figure 1b) and spectral bandwidths (Figure 1c).

Gold Nanorods of Different Sizes Exhibit Unique Stability Trends

It is critical for (L)GNRs to remain stable through multiple washes so that cytotoxic CTAB can be removed and the particles can be further functionalized for biological use. As expected based on previous reports,[30,32] (L)GNRs-CTAB synthesized by either method aggregated after minimal washing by centrifugation (Figure 2a–e and Figures S2 and S3). LGNRs-CTAB aggregated after two rounds of washing while GNRs-CTAB aggregated after three rounds. While GNRs-mPEG remained stable for an additional wash relative to GNRs-CTAB, LGNRs-mPEG experienced no such increase in stability relative to LGNRs-CTAB. This suggested that LGNRs did not benefit from mPEG coating. Unlike LGNRs-mPEG, LGNRs-PSS exhibited marked improvements in stability, remaining stable for more than four washes. Long-term particle stability (“shelf-life”) is also an important practical consideration. We found that LGNRs-PSS stored at 4 °C were stable for more than a year (Figure S11).

Zeta potential measurements (Figure 2f and Figure S4, Table S1) indicated a rapid shift from positive to negative surface potential for LGNRs-CTAB incubated with PSS, which led to increased stability consistent with polyelectrolytic overcoating.[31,32] In contrast, the zeta potentials of LGNRs-CTAB and LGNRs-mPEG were positive, but tended toward zero as observed for GNRs-CTAB and GNRs-mPEG. Despite the similarities in stability and zeta potential for LGNRs-CTAB and LGNRs-mPEG, later studies indicated that PEG-SH reagents do successfully bind LGNRs to provide particle coating. We did not observe

spectral broadening for LGNRs upon addition of PSS or after washing. These findings indicated that conventional PEG-based methods for GNR surface coating were insufficient to confer stability in aqueous solutions for GNRs of different sizes. However, PSS could be used successfully to stabilize LGNRs in water.

We wanted to understand why PEG-SH stabilized GNRs but not LGNRs. Based on previous studies of PEG-SH to GNRs,[33–37] we hypothesized that the stability difference between GNRs and LGNRs arose from the specific locations of PEG-SH binding on the (L)GNR surface. Specifically, we expected that those binding sites influenced the extent to which PEG can cover the (L)GNR surface. To address these differences, we added mPEG-SH to GNRs-CTAB and observed that the particles underwent plasmonic red-shifting (~20 nm), and LGNRs-CTAB incubated with PSS exhibited blue-shifting (~10 nm). Both of these shifts suggested successful surface modification (Figure S5). While LGNRs-mPEG exhibited no significant change in plasmonic resonance relative to LGNRs-CTAB, an increase in hydrodynamic diameter of ~10 nm was observed for LGNRs-CTAB following mPEG-SH incubation (Table S2), indicating successful mPEG-SH conjugation. Next, we sought to explore where PEG-SH reagents bind to (L)GNR surfaces. To study this, LGNRs-CTAB and GNRs-CTAB were incubated with Biotin-PEG-SH to produce LGNRs-PEG-Biotin and GNRs-PEG-Biotin, respectively. We then attached 10 nm NeutrAvidin-coated gold nanospheres (GNS-NA) to LGNRs-PEG-Biotin (see Supporting Results for more details). TEM images showed that GNS-NA localized preferentially to the end-caps of LGNRs-PEG-Biotin, but no such pattern was observed when GNS-NA were incubated with LGNRs-mPEG (Figure S6). This confirmed our hypothesis that PEG-SH reagents bound primarily to the end-caps of (L)GNRs. LGNRs-mPEG incubated with GNS-NA exhibited partial aggregation as observed by TEM, spectral broadening, and DLS, indicative of instability. However, LGNRs-PEG-Biotin remained stable, and they experienced ~20 nm red-shifting and increased hydrodynamic diameter after GNS-NA incubation (Figures S6–7, Table S3), consistent with an effective increase in particle aspect ratio due to GNS binding at LGNR end-caps (for more information, see Supporting Results).

Biostability of LGNRs

Absorbance measurements indicated that LGNRs-PSS remained stable during and after incubation with FBS followed by washing (Figure 3a, see detailed Experimental Section). Interestingly, LGNRs-mPEG incubated with FBS were stable after two washes while LGNRs-mPEG in water were stable for only one wash. It is likely that adsorbed FBS (the so-called “protein corona”) is responsible for this extended stability. Spectral broadening occurred after the third wash for LGNRs-mPEG but not for LGNRs-PSS (Figure 3b,c). This result showed that, while LGNRs-mPEG aggregated, LGNRs-PSS remained stable even after excess FBS was washed away. Furthermore, we qualitatively observed no adverse effects or behavioral changes in female nude (nu^{-}/nu^{-}) and C57BL/6 mice ($n = 5$) up to three months after intravenous administration of LGNRs-PSS-mPEG. These observations suggest that, in addition to being biostable, LGNRs-PSS-mPEG can be used safely in animal experiments. Ex vivo analysis of resected mouse tissues further indicated the in vivo stability of LGNRs-PSS-mPEG (Figure S12).

LGNR Functionalization for Specific Ligand–Receptor Binding

Several previous reports describe conjugation of antibodies to GNRs-PSS through electrostatic adsorption.[1,7,10,31] However, covalent chemistry and high-affinity biomolecule interactions are favorable because they are more stable than electrostatic adhesions in biological fluids. Furthermore, specific chemistry can be used to bind biomolecules such as antibodies at specific functional groups rather than generic electrostatic patches. We therefore tested methods to conjugate biological molecules to LGNRs-PSS through specific interactions. Because of the high affinity interaction between biotin and streptavidin, we hypothesized that LGNRs-PSS-PEG-Biotin would bind to the beads, whereas LGNRs-PSS-mPEG would remain free in solution (Figure 4a, “Binding Assay”). After 20 s of centrifugation at 1000*g*, a dark red pellet of LGNRs-PSS-PEG-Biotin and streptavidin beads was observed, and the color of the supernatant was markedly clear, indicating an absence of free LGNRs-PSS-PEG-Biotin in solution. In contrast, the pellet from the LGNRs-PSS-mPEG incubation was white (the color of beads only) and the supernatant from this incubation remained very red, indicating the presence of GNRs in solution (Figure S8a). After washing beads postincubation, a clear difference in bead pellet color was observed for streptavidin beads incubated with LGNRs-PSS-PEG-Biotin versus LGNRs-PSS-mPEG in FBS (Figure S8b). This difference indicated that LGNRs-PSS-PEG-Biotin bound with specificity to streptavidin coated beads even in the presence of FBS while LGNRs-PSS-mPEG do not. Furthermore, blocking the streptavidin-coated beads with free biotin prior to GNR incubation (Figure 4a, “Blocking Assay”) prevented LGNRs-PSS-PEG-Biotin binding (note the lack of red color in the pellet). The LGNRs-PSS-mPEG result remained the same as in the unblocked condition (Figure S8b). To confirm visual assessments of each assay, we measured absorbance spectra for supernatants from blocked and unblocked incubation conditions. Despite using equivalent amounts of GNRs in each incubation, a much higher concentration of LGNRs-PSS-mPEG remained in solution compared to LGNRs-PSS-PEG-Biotin. This result indicated that more LGNRs-PSS-PEG-Biotin were removed from solution (i.e., bound to beads) than LGNRs-PSS-mPEG. However, preincubation of the streptavidin beads with free biotin prevented this effect (Figure 4b), suggesting that the observed interaction of LGNRs-PSS-PEG-Biotin and streptavidin beads was molecularly specific. The results of the binding and blocking assays collectively indicated that 1) PEG-SH reagents are capable of binding the surface of LGNRs-PSS and 2) heterobifunctional PEG molecules (e.g., Biotin-PEG-SH) can be conjugated to LGNRs-PSS to enable subsequent specific conjugation with biological ligands of interest, even in the presence of nonspecific proteins.

We further explored LGNR bioconjugation by preparing LGNRs-PSS-coated with cyclic RGD (cRGD), a peptide that binds with high affinity to $\alpha_V\beta_3$ integrin, a cell-surface receptor overexpressed by numerous cancer cell lines. Dark-field spectral microscopy revealed that U87MG cells (which are $\alpha_V\beta_3^+$) exhibited greater uptake of LGNRs targeted with cRGD compared to uptake of LGNRs-mPEG or LGNRs functionalized with the low-affinity control peptide, cRAD (Figures S13, see Detailed Experimental Methods in Supporting Information).

Optical Advantages of LGNRs

In addition to developing methods to prepare LGNRs for biological applications, we sought to demonstrate the favorable optical properties of LGNRs relative to conventional GNRs. LGNRs (2×10^{10} nps/mL) exhibited an intense OCT signal compared to GNRs at the same concentration, which were barely distinguishable above the system's noise threshold ($p < 0.0001$; Figure 5a, Figures S9–10). In order to accurately compare the OCT signals of LGNRs and GNRs, we also scanned GNRs at an 8-fold higher concentration (1.6×10^{11} nps/mL), which produce the same optical density (OD) as LGNRs prepared at 2×10^{10} nps/mL. Even at this 8× higher concentration, the OCT signal of GNRs was only ~¼ that of the LGNRs signal ($p < 0.0001$; Figure 5b), suggesting that LGNRs produce ~32-fold greater OCT signal than GNRs per particle. We were also able to detect individual LGNRs with OCT, enabling single-particle imaging sensitivity in vitro (Figure 5c). Consistent with theoretical predictions, this result suggested that scattering constitutes a greater proportion of the total absorbance of LGNRs versus GNRs, making LGNRs an excellent OCT contrast agent. Together, the scattering and absorbance measurements indicated that GNRs may be replaced with LGNRs in existing biomedical studies for greatly enhanced optical effects.

LGNR Enhancement of in Vivo Imaging

Contrast sensitivity is critical for observing fine details in biological samples, especially deep within intact tissue. We wanted to test whether the strong optical signal from LGNRs could improve OCT imaging sensitivity for *in vivo* studies. Due to scattering and absorption, OCT has a limited imaging depth, which typically prevents the detection of fine structures more than a few hundred microns into intact tissue. However, IV-administered LGNRs-PSS-mPEG produced enough backscattering to provide strong contrast enhancement in blood vessels, particularly in small vessels (<100 μm in diameter) over 500 μm deep within the tumor. In this case, the contrast from LGNRs-PSS-mPEG enabled detection of vasculature at twice the depth achievable with OCT alone (Figure 5d).

4. DISCUSSION

Perhaps the most interesting finding from this study is that GNRs of larger-than-conventional sizes cannot be sufficiently stabilized by one of the most commonly implemented surface modification methods (PEGylation). This result is consistent with previous reports that describe a decrease in gold nanosphere stability with increasing size.[38–40] Our results show that PEG-SH binding occurs mostly at the ends of (L)GNRs, which agree with previous reports detailing how nanorod synthesis conditions lead to face-dependent PEG-SH binding.[36–40] Specifically, PEG-SH reagents preferentially bind to the end-caps of (L)GNRs while the longitudinal faces remain largely coated with excess CTAB from synthesis. CTAB is removed through multiple wash steps, leaving only the (L)GNR end-caps protected with a PEG coating. It is interesting to note that the maximum outstretched length of PEG-SH reagents with MW ~ 5 kDa is ~50 nm, and the persistence length in solution is expected to be ~25 nm.[41] This persistence length implies that bundled PEG chains anchored by Au–S bonds to both GNR end-caps may still provide stabilization to a significant portion of the GNR longitudinal surface. Because LGNRs have greater lengths than GNRs, end-bound PEG-SH reagents at persistence length likely do not provide

sufficient coating of the longitudinal surface area after CTAB is washed away. This surface area exposure may ultimately lead to earlier particle aggregation when compared to GNRs-mPEG. Unlike PEG-SH, PSS binding to LGNRs-CTAB is not limited to the end-caps. The anions in PSS can bind CTAB cationic head groups across the LGNRs-CTAB surface to provide a more thorough particle overcoating. Even if CTAB is washed away, the GNR surface remains wrapped in the large (~70 kDa) polyanion. Additionally, LGNRs-PSS are expected to remain stable in solution due to strong interparticle electrostatic repulsion. This repulsion is expected to be more effective than inter-GNR steric hindrance provided by PEG-SH (for more information, see Supporting Information). Interestingly, a previous study by Mehtala and Wei suggests that small GNRs coated with PSS form minor aggregates that are detectable through single-nanoparticle tracking methods (LGNRs were not tested). However, the detected aggregates did not produce observable changes to the Vis-NIR spectra of GNRs-PSS relative to fully dispersed GNRs.[42] The use of PSS to coat the surface of extremely long gold nanoparticles (>400 nm) has previously been reported, however the biostability and in vivo use of these particles was not evaluated.[43] Moreover, particles with such extreme high aspect ratios may be unsuitable for live animal applications due to shape-dependent toxicity and poor cellular uptake (similar to effects observed for carbon nanotubes).[44,45] Thus, the biofunctionalized LGNRs reported herein alleviate a technological gap between small (<50 nm), low-signal particles and exceedingly large (>200 nm), potentially toxic particles.

LGNRs-PSS are also stable in biological conditions. This is based on our observations that LGNRs-PSS incubated with FBS remained highly stable and that intravenous injection of LGNRs led to visible increases in OCT contrast (which relies on retention of particle spectral properties and thus particle stability). Furthermore, LGNRs-PSS-mPEG caused no signs of distress in nude (nu^{-}/nu^{-}) or C57BL/6 mice, indicating that these particles are suitable for use in live animals.

A highly advantageous characteristic for any biomedical nanoparticle is the ability to bind specific molecular targets of interest. Molecular specificity is enabled by the use of a surface coating that can be further conjugated with biological ligands or antibodies. Ideally, molecular targeting moieties can be linked to the nanoparticle through covalent bonds or high-affinity biomolecular interactions. Our proof of concept binding experiments with LGNRs-PSS-PEG-Biotin and streptavidin beads and targeted cell incubation experiments show that LGNRs-PSS can be functionalized with such biological ligands. Through this demonstration, we have developed LGNRs as a versatile platform for producing molecularly targeted contrast agents.

Our comparison of GNR and LGNR OCT signals empirically demonstrates a key benefit of LGNRs for future applications in biomedicine. Consistent with theory and simulation,[25,26] LGNRs scatter significantly more light than GNRs, making them ideal agents for scattering-based imaging modalities. While small GNRs have been demonstrated for OCT contrast enhancement,[18] the ability to identify individual LGNRs described in this report realizes a new level of OCT imaging sensitivity. Spectral domain OCT contrast enhancement can also be optimized by selecting LGNRs with a plasmonic peak that overlaps strongly with the OCT illumination source and detection range.

Practical advantages of increased imaging sensitivity from LGNR increased scattering include the detection of fine anatomical structures with in vivo OCT imaging. The several hundred micron increase in imaging depth enabled by LGNR contrast may offer technical improvements for OCT investigations of skin lesions, particularly in distinguishing benign from growing malignant tumors through identification of angiogenesis.

Because the total interaction with light is greater for LGNRs than conventional GNRs, we expect that LGNRs may enable similar enhancements for other near-infrared imaging techniques that use GNRs. Small GNRs-mPEG produced using the Murray method have been used for deep-tissue three-photon luminescence imaging in mice.[46] The use of LGNRs-PSS may further improve the achievable sensitivity and depth of luminescence imaging techniques owing to greater per particle photon interaction. Surface-enhanced raman scattering (SERS) is another imaging technique that commonly relies on GNRs to increase the signals of Raman-active dyes. While not in the scope of this report, future SERS comparisons of GNR and LGNR signal enhancement may reveal additional biosensing application for the functionalized LGNRs reported herein.

5. CONCLUSION

In summary, this work not only underscores the relation between nanoparticle size and stability but also offers immediate improvements to current biological studies that use gold nanorod contrast agents. LGNRs are not stabilized by the steric effects through which PEG chains improve the stability of GNRs. Unlike GNRs, LGNRs may require stabilization through stronger electrostatic repulsive interactions among particles. More importantly, this work has demonstrated the practical benefits of understanding LGNR stability. From an applications-based standpoint, it is critical to note that LGNRs (and perhaps other types of nanoparticles) must be functionalized using tailored surface chemistry methods if their advantages in biomedical imaging and therapy are to be realized. In achieving one such tailored approach, we have developed improved functionalized nanoparticles that can provide immediate enhancements in detection sensitivity for contrast-enhanced imaging and biosensing techniques that currently rely on conventional GNRs.

Supplementary Material

Refer to Web version on PubMed Central for supplementary material.

Acknowledgments

We thank the Cell Sciences Imaging Facility (CSIF) at Stanford for use of the JEOL TEM (NIH SIG #1S10RR026780001). E.S. acknowledges funding from the Stanford Biophysics Program training grant (T32 GM-08294). O.L. is grateful for a Stanford Bowes Bio-X Graduate Fellowship. A.D. is a Pew-Stewart Scholar for Cancer Research supported by The Pew Charitable Trusts and The Alexander and Margaret Stewart Trust. We thank Tim Larson, Jesse Jokerst, and Erez Podoly for their advice on GNR synthesis, and we extend special thanks to Roopa Dalal for tissue sectioning and staining. We also thank Dr. Sanjiv Sam Gambhir for access to the Malvern ZetaSizer instrument. This work was funded in part by grants from the United States Air Force (FA9550-15-1-0007), the National Institute of Health (NIH DP50D012179), the National Science Foundation (NSF 1172802-100-QAANU), the Damon Runyon Cancer Research Center (DFS# 06-13), the Susan G. Komen Breast Cancer Foundation (SAB15-00003), the Mary Kay Foundation, the Donald E. and Delia B. Baxter Foundation, the Claire Giannini Fund, the Skippy Frank Foundation, a seed grant from the Center for Cancer Nanotechnology Excellence and Translation (CCNE-T U54CA151459), a seed grant from the Stanford Nano Center (SNC) and

Stanford Nanocharacterization Lab (SNL) for GNR characterization, and a Stanford Bio-X Interdisciplinary Initiative Seed Grant.

ABBREVIATIONS

GNRs	gold nanorods
LGNRs	large gold nanorods
CTAB	cetyltrimethylammonium bromide
mPEG	methoxy-polyethylene glycol
PSS	polystyrenesulfonate
TEM	transmission electron microscopy
Vis-NIR	visible-near-infrared
OCT	optical coherence tomography
DLS	dynamic light scattering
FWHM	full width at half-maximum

REFERENCES

1. Huang X, El-Sayed IH, Qian W, El-Sayed MA. Cancer Cell Imaging and Photothermal Therapy in the Near-Infrared Region by Using Gold Nanorods. J. Am. Chem. Soc. 2006; 128:2115–2120. [PubMed: 16464114]
2. Hauck TS, Jennings TL, Yatsenko T, Kumaradas JC, Chan WCW. Enhancing the Toxicity of Cancer Chemotherapeutics with Gold Nanorod Hyperthermia. Adv. Mater. 2008; 20:3832–3838.
3. von Maltzahn G, Park JH, Agrawal A, Bandaru NK, Das SK, Sailor MJ, Bhatia SN. Computationally Guided Photothermal Tumor Therapy Using Long-Circulating Gold Nanorod Antennas. Cancer. Res. 2009; 69:3892–3900. [PubMed: 19366797]
4. Huang HC, Barua S, Kay DB, Rege K. Simultaneous Enhamcenent of Photothermal Stability and Gene Delivery Efficacy of Gold Nanorods Using Polyelectrolytes. ACS Nano. 2009; 3:2941–2952. [PubMed: 19856978]
5. Choi WI, Kim JY, Kang C, Byeon CC, Kim YH, Tae G. Tumor Regression in vivo by Photothermal Therapy Based on Gold-Nanorod-Loaded, Functional Nanocarriers. ACS Nano. 2011; 5:1995–2003. [PubMed: 21344891]
6. Pissuwan D, Valenzuela SM, Cortie MB. Prospects for Gold Nanorod Particles in Diagnostic and Therapeutic Applications. Biotechnol. Genet. Eng. Rev. 2008; 25:93–112. [PubMed: 21412351]
7. Durr NJ, Larson T, Smith DK, Korgel BA, Sokolov K, Ben-Yakar A. Two-Photon Luminescence Imaging of Cancer Cells Using Molecularly Targeted Gold Nanorods. Nano Lett. 2007; 7:941–945. [PubMed: 17335272]
8. Wang H, Huff TB, Zweifel DA, He W, Low PS, Wei A, Cheng JX. In vitro and in vivo Two-Photon Luminescence Imaging of Single Gold Nanorods. Proc. Natl. Acad. Sci. U. S. A. 2005; 102:15752–15756. [PubMed: 16239346]
9. Tong L, He W, Zhang Y, Zheng W, Cheng JX. Visualizing Systemic Clearance and Cellular Level Biodistribution of Gold Nanorods by Intrinsic Two-Photon Luminescence. Langmuir. 2009; 25:12454–12459. [PubMed: 19856987]
10. Huang X, El-Sayed IH, Qian W, El-Sayed MA. Cancer Cells Assemble and Align Gold Nanorods Conjugated to Antibodies to Produce Highly Enhanced, Sharp, and Polarized Surface Raman

Spectra: A Potential Cancer Diagnostic Marker. Nano Lett. 2007; 7:1591–1597. [PubMed: 17474783]

11. von Maltzahn G, Centrone A, Park JH, Ramanathan R, Sailor MJ, Hatton TA, Bhatia SN. SERS-Coded Gold Nanorods as a Multifunctional Platform for Densely Multiplexed Near-Infrared Imaging and Photothermal Heating. Adv. Mater. 2009; 21:3175–3180. [PubMed: 20174478]
12. Qian J, Jiang L, Cai F, Wang D, He S. Fluorescence-Surface Enhanced Raman Scattering Co-Functionalized Gold Nanorods as Near-Infrared Probes for Purely Optical in vivo Imaging. Biomaterials. 2011; 32:1601–1610. [PubMed: 21106233]
13. Zijlstra P, Paulo PMR, Orrit M. Optical Detection of Single Non-Absorbing Molecules Using the Surface Plasmon Resonance of a Gold Nanorod. Nat. Nanotechnol. 2012; 7:379–382. [PubMed: 22504707]
14. Agarwal A, Huang SW, O'Donnell M, Day KC, Day M, Kotov N, Ashkenazi S. Targeted Gold Nanorod Contrast Agent for Prostate Cancer Detection by Photoacoustic Imaging. J. Appl. Phys. 2007; 102:064701.
15. Chen YS, Frey W, Kim S, Kruizinga P, Homan K, Emelianov S. Silica-Coated Gold Nanorods as Photoacoustic Signal Nanoamplifiers. Nano Lett. 2011; 11:348–354. [PubMed: 21244082]
16. Jokerst JV, Thangaraj M, Kempen P, Sinclair R, Gambhir SS. Photoacoustic Imaging of Mesenchymal Stem Cells in Living Mice via Silica-Coated Gold Nanorods. ACS Nano. 2012; 6:5920–5930. [PubMed: 22681633]
17. Jokerst JV, Cole AJ, Van de Sompel D, Gambhir SS. Gold Nanorods for Ovarian Cancer Detection with Photoacoustic Imaging and Resection Guidance via Raman Imaging in Living Mice. ACS Nano. 2012; 6:10366–10377. [PubMed: 23101432]
18. Oldenburg AL, Hansen MN, Zweifel DA, Wei A, Boppart SA. Plasmon-Resonant Gold Nanorods as Low Backscattering Albedo Contrast Agents for Optical Coherence Tomography. Opt. Express. 2006; 14:6724–6738. [PubMed: 19516854]
19. Tucker-Schwartz JM, Meyer TA, Patil CA, Duvall CL, Skala MC. In vivo Photothermal Optical Coherence Tomography of Gold Nanorod Contrast Agents. Biomed. Opt. Express. 2012; 3:2881–2895. [PubMed: 23162726]
20. Yu YY, Chang SS, Lee CL, Wang CRC. Gold Nanorods: Electrochemical Synthesis and Optical Properties. J. Phys. Chem. B. 1997; 101:6661–6664.
21. Jana NR, Gearheart L, Murphy CJ. Wet Chemical Synthesis of High Aspect Ratio Cylindrical Gold Nanorods. J. Phys. Chem. B. 2001; 105:4065–4067.
22. Kim F, Song JH, Yang P. Photochemical Synthesis of Gold Nanorods. J. Am. Chem. Soc. 2002; 124:14316–14317. [PubMed: 12452700]
23. Nikoobakht B, El-Sayed MA. Preparation and Growth Mechanism of Gold Nanorods (NRs) Using Seed-Mediated Growth Method. Chem. Mater. 2003; 15:1957–1962.
24. Ye X, Zheng C, Chen J, Gao Y, Murray CB. Using Binary Surfactant Mixtures to Simultaneously Improve the Dimensional Tunability and Monodispersity in the Seeded Growth of Gold Nanorods. Nano Lett. 2013; 13:765–771. [PubMed: 23286198]
25. Lee KS, El-Sayed MA. Dependence of the Enhanced Optical Scattering Efficiency Relative to that of Absorption for Gold Metal Nanorods on Aspect Ratio, Size, End-Cap Shape, and Medium Refractive Index. J. Phys. Chem. B. 2005; 109:20331–20338. [PubMed: 16853630]
26. Jain PK, Lee KS, El-Sayed IH, El-Sayed MA. Cacluated Absorption and Scattering Properties of Gold Nanoparticles of Different Size, Shape, and Composition: Applications in Biological Imaging and Biomedicine. J. Phys. Chem. B. 2006; 110:7238–7248. [PubMed: 16599493]
27. Prescott SW, Mulvaney P. Gold Nanorod Extinction Spectra. J. Appl. Phys. 2006; 99:123504.
28. Ni W, Kou X, Yang Z, Wang J. Tailoring Longitudinal Surface Plasmon Wavelengths, Scattering and Absorption Cross Sections of Gold Nanorods. ACS Nano. 2008; 2:677–686. [PubMed: 19206598]
29. Niidome T, Yamagata M, Okamoto Y, Akiyama Y, Takahashi H, Kawano T, Katayama Y, Niidome Y. PEG-Modified Gold Nanorods with a Stealth Character for in vivo Applications. J. Controlled Release. 2006; 114:343–347.
30. Rostro-Kohanloo BC, Bickford LR, Payne CM, Day ES, Anderson LJE, Zhong M, Lee S, Mayer KM, Zal T, Adam L, Dinney CPN, Drezek RA, West JL, Hafner JH. The Stabilization and

Targeting of Surfactant-Synthesized Gold Nanorods. Nanotechnology. 2009; 20:434005. [PubMed: 19801751]

31. Parab HJ, Chen HM, Lai TC, Huang JH, Chen PH, Liu RS, Hsiao M, Chen CH, Tsai DP, Hwu YK. Biosensing, Cytotoxicity, and Cellular Uptake Studies of Surface-Modified Gold Nanorods. J. Phys. Chem. C. 2009; 113:7574–7578.
32. Rayavarapu RG, Petersen W, Hartsuiker L, Chin P, Janssen H, van Leeuwen FWB, Otto C, Manohar S, van Leeuwen TG. In vitro toxicity studies of Polymer-Coated Gold Nanorods. Nanotechnology. 2010; 21:145101. [PubMed: 20220222]
33. Nikoobakht B, El-Sayed MA. Evidence for Bilayer Assembly of Cationic Surfactants on the Surface of Gold Nanorods. Langmuir. 2001; 17:6368–6374.
34. Gao J, Bender CM, Murphy CJ. Dependence of the Gold Nanorod Aspect Ratio on the Nature of the Directing Surfactant in Aqueous Solution. Langmuir. 2003; 19:9065–9070.
35. Caswell KK, Wilson JN, Bunz UHF, Murphy CJ. Preferential End-to-End Assembly of Gold Nanorods by Biotin-Streptavidin Connectors. J. Am. Chem. Soc. 2003; 125:13914–13915. [PubMed: 14611200]
36. Pérez-Juste J, Pastoriza-Santos I, Liz-Marzá'n LM, Mulvaney P. Gold Nanorods: Synthesis, Characterization, and Applications. Coord. Chem. Rev. 2005; 249:1870–1901.
37. Nie Z, Fava D, Rubinstein M, Kumacheva E. Supramolecular" Assembly of Gold Nanorods End-Terminated with Polymer "pom-poms": effect of pom-pom structure on the association modes. J. Am. Chem. Soc. 2008; 130:3683–3689. [PubMed: 18298120]
38. Mallick K, Wang ZL, Pal T. Seed-Mediated Successive Growth of Gold Particles Accomplished by UV Irradiation: a Photochemical Approach for Size-Controlled Synthesis. J. Photochem. Photobiol., A. 2001; 140:75–80.
39. Jana NR, Gearheart L, Murphy CJ. Seeding Growth for Size Control of 5–40 nm Diameter Gold Nanoparticles. Langmuir. 2001; 17:6782–6786.
40. Perrault SD, Chan WCW. Synthesis and Surface Modification of Highly Monodispersed, Spherical Gold Nanoparticles of 50–200 nm. J. Am. Chem. Soc. 2009; 131:17042–17043. [PubMed: 19891442]
41. Choi CHJ, Zuckerman JE, Webster P, Davis ME. Targeting Kidney Mesangium by Nanoparticles of Defined Size. Proc. Natl. Acad. Sci. U. S. A. 2011; 108:6656–6661. [PubMed: 21464325]
42. Mehtala JG, Wei A. Nanometric Resolution in the Hydrodynamic Size Analysis of Ligand-Stabilized Gold Nanorods. Langmuir. 2014; 30:13737–13743. [PubMed: 25349895]
43. Gole A, Murphy CJ. Polyelectrolyte-Coated Gold Nanorods: Synthesis, Characterization, and Immobilization. Chem. Mater. 2005; 17:1325–1330.
44. Poland CA, Duffin R, Kinloch I, Maynard A, Wallace WAH, Seaton A, Stone V, Brown S, MacNee W, Donaldson K. Carbon Nanotubes Introduced into the Abdominal Cavity of Mice Show Asbestos-Like Pathogenicity in a Pilot Study. Nat. Nanotechnol. 2008; 3:423–428. [PubMed: 18654567]
45. Alkilany AM, Murphy CJ. Toxicity and Cellular Uptake of Gold Nanoparticles: What Have we Learned so Far? J. Nanopart. Res. 2010; 12:2313–2333. [PubMed: 21170131]
46. Wang S, Xi W, Cai F, Zhao X, Xu Z, Qian J, He S. Three-Photon Luminescence of Gold Nanorods and its Application for High Contrast Tissue and Deep in vivo Brain Imaging. Theranostics. 2015; 5:251–266. [PubMed: 25553113]

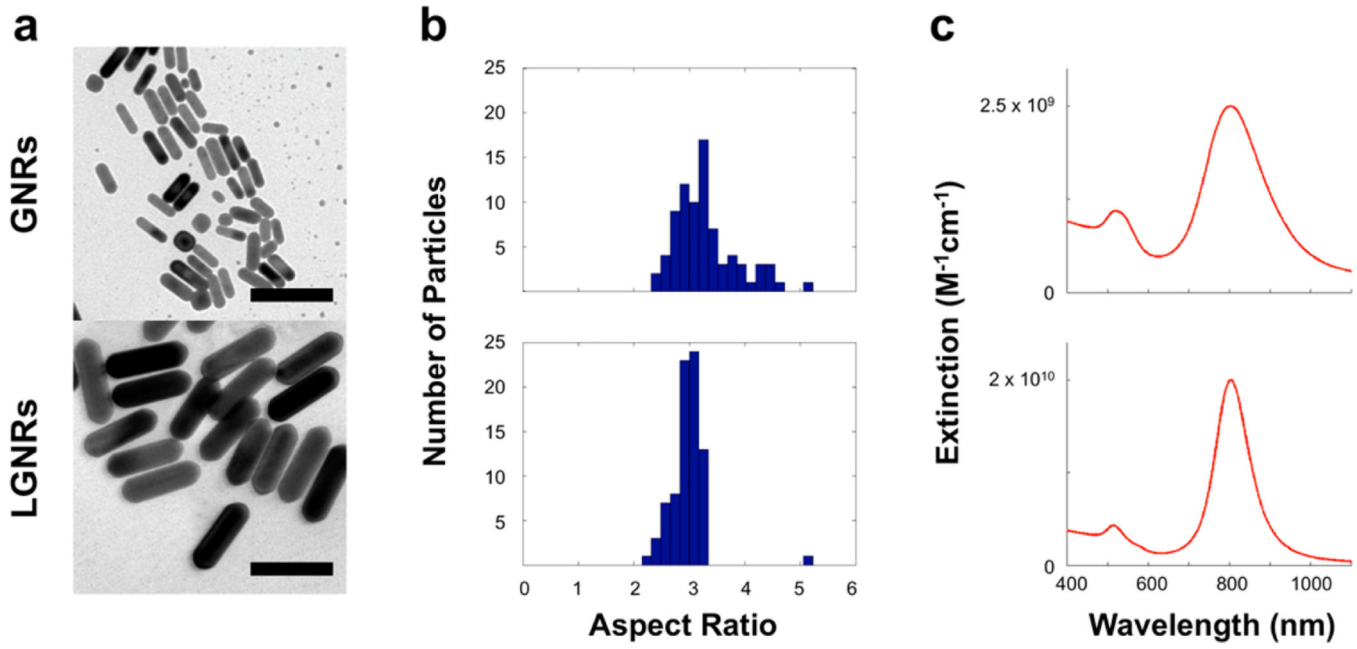

Figure 1.

Initial particle characterization. (a) TEM images of GNRs (length: 45 ± 7 nm, width: 14 ± 2 nm) and LGNRs (length: 93 ± 7 nm, width: 33 ± 1 nm) produced by separate methods (scale bars = 100 nm). Additional TEM images are provided in Figure S1. (b) Particle aspect ratio (AR) distributions for GNR and LGNR batches (n = 80 for each) were determined. GNRs AR: 3.3 ± 0.6, and LGNRs AR: 3.0 ± 0.3. (c) Absorbance spectra of each GNR batch were also measured. GNRs peak wavelength: 802 nm, and LGNRs peak wavelength: 804 nm. LGNRs exhibited a narrower spectrum (FWHM = 100 nm) than GNRs (FWHM = 150 nm).

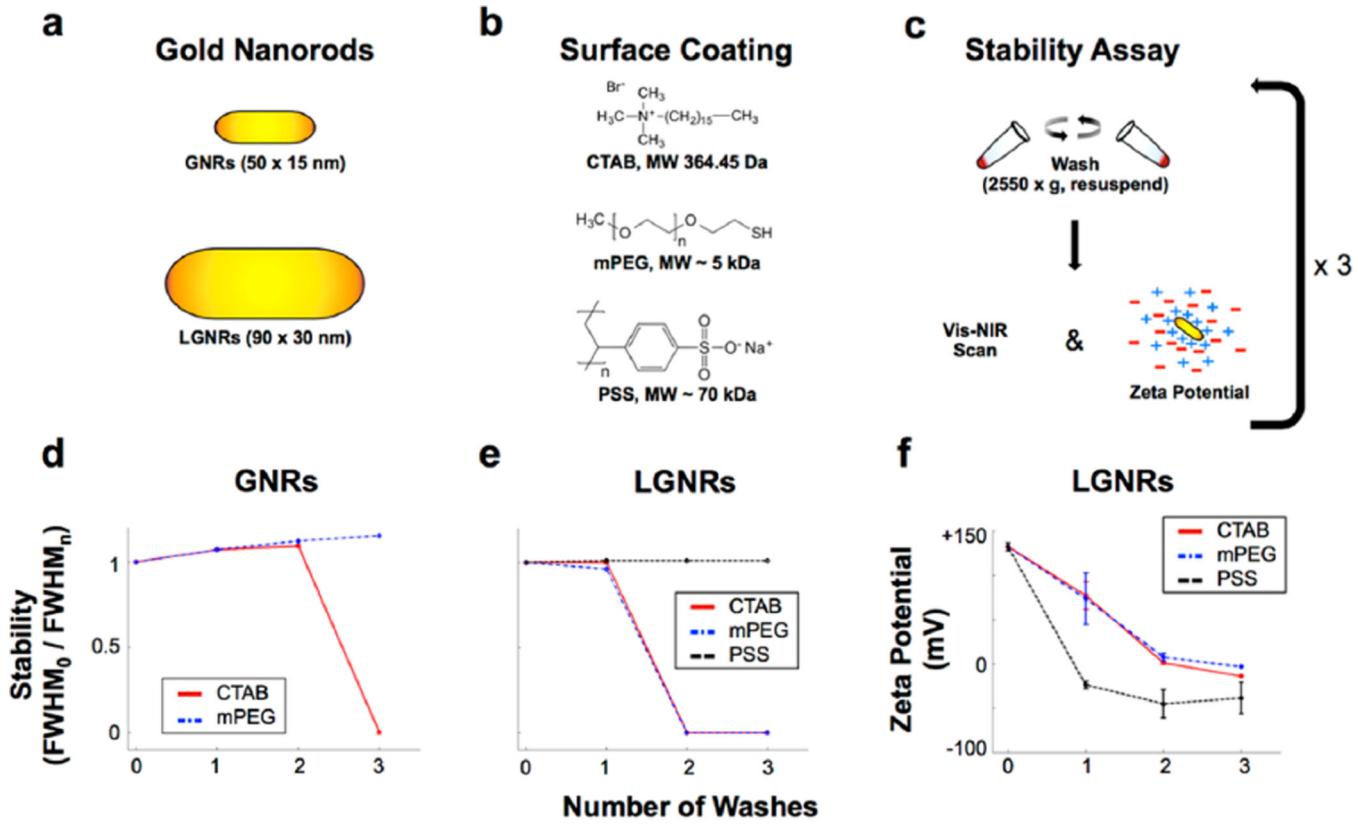

Figure 2.

Characterization of GNR stability trends as a function of size and surface coating. (a,b) GNRs and LGNRs were initially characterized by Vis-NIR spectrometry and Electrophoretic Light Scattering (ELS) and subsequently prepared with one of three different surface coating molecules. (c) Coated GNRs were then subjected to consecutive rounds of washing with distilled deionized water and centrifugation. GNRs were analyzed by Vis-NIR spectrometry and ELS after each wash to evaluate particle stability. (d,e) Particle stability was measured as spectral peak broadening by dividing the longitudinal absorbance peak full width at half-maximum before washing ($FWHM_0$) by peak full width at half-maximum after each of the washes ($FWHM_n$, where $n = 0–3$). Plotting $FWHM_0/FWHM_n$ for each GNR size and coating reveals trends in stability for comparison. Original absorbance spectra for all GNRs are presented in Figures S2 and S3. (f) Zeta potential measurements for LGNRs are consistent with spectral stability trends, and they also provide validation of successful surface coating. Error bars represent standard error of the mean (s.e.m.) from triplicate measurements. Zeta potential measurements for all GNRs are presented in Figure S4 and Table S1.

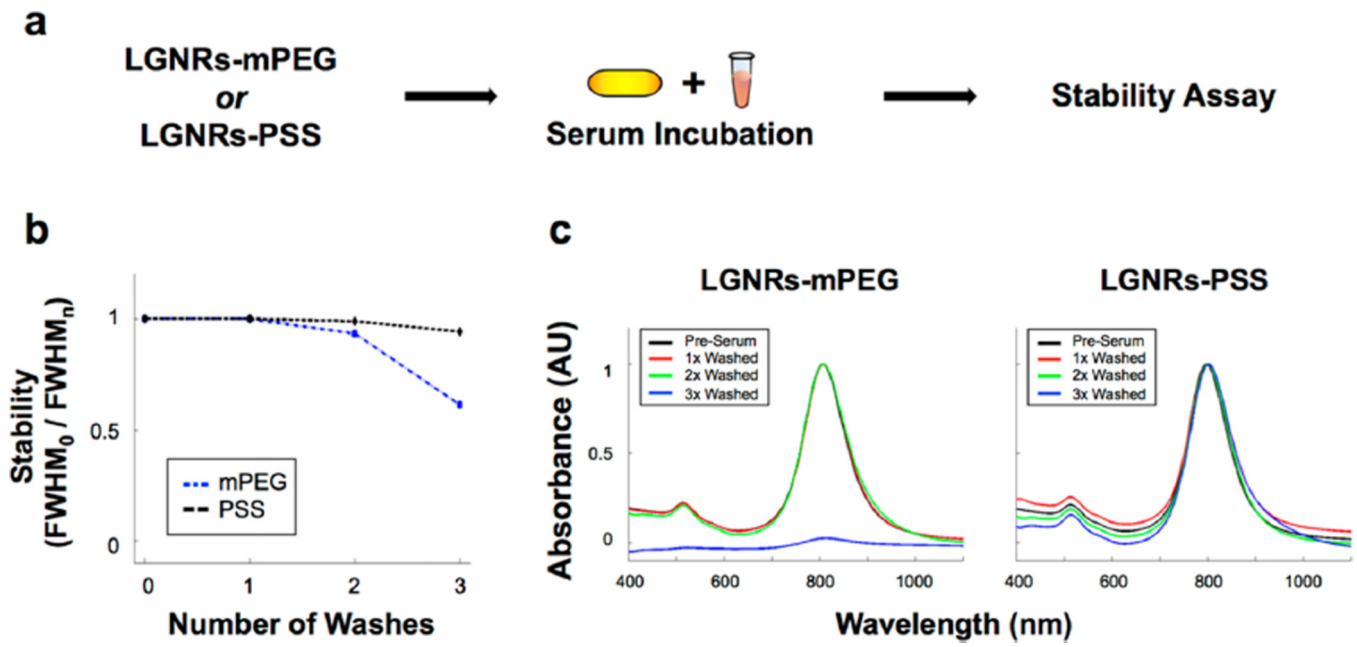

Figure 3.

LGNRs are robustly stable in biological serum. (a) LGNRs-mPEG and LGNRs-PSS were prepared, incubated with fetal bovine serum (FBS) for 3 h, and subjected to three rounds of washing by centrifugation. (b) The normalized absorbance spectrum of each GNR type was taken after each wash to assess serum stability. Measurements of absorbance peak $FWHM_0$/$FWHM_n$ demonstrate that LGNRs-PSS are more stable in biological serum than LGNRs-mPEG. (c) Raw absorbance spectra for each particle type demonstrate this difference in stability more clearly, as LGNRs-mPEG exhibit virtually no plasmonic peak after the third wash. Unlike LGNRs-mPEG, LGNRs-PSS exhibit little change in absorbance properties.

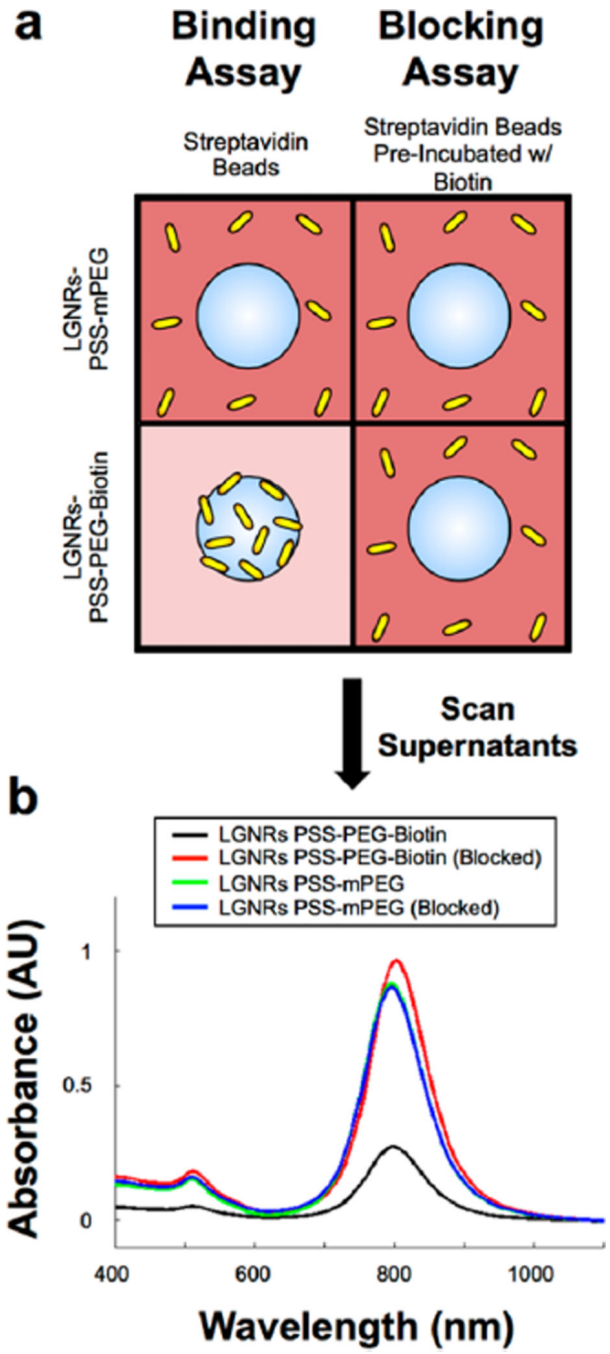

Figure 4.

LGNRs-PSS can be subsequently functionalized to achieve high-specificity molecular binding properties. (a) LGNRs-PSS-PEG-Biotin and LGNRs-PSS-mPEG were prepared and incubated with FBS to mimic biological environments. FBS-incubated GNRs were then used in biotin–streptavidin binding and blocking assays. For the binding assay, LGNRs-PSS-PEG-Biotin and LGNRs-PSS-mPEG were incubated with streptavidin-coated polystyrene beads (3 μm diameter) and centrifuged for 10s at 1000*g* to separate beads from free GNRs. The same process was repeated in the blocking assay, except that the streptavidin-coated

beads were preincubated with excess free biotin to preclude specific binding of Large-GNRs-PSS-PEG-Biotin. (b) Absorbance measurements of the supernatant from each of the four bead-GNR combinations were taken after incubation. The same concentration of GNRs (OD 1) was used in each incubation, but only the supernatants from the incubation of LGNRs-PSS-PEG-Biotin and streptavidin beads exhibited a significant decrease in GNR concentration. These results demonstrate the proof of principle that LGNRs-PSS can be functionalized with ligands that retain molecular binding specificity in the presence of nonspecific proteins, which will be advantageous for future applications to targeted molecular imaging. Photographs from these molecular specificity assays are presented in Figure S5.

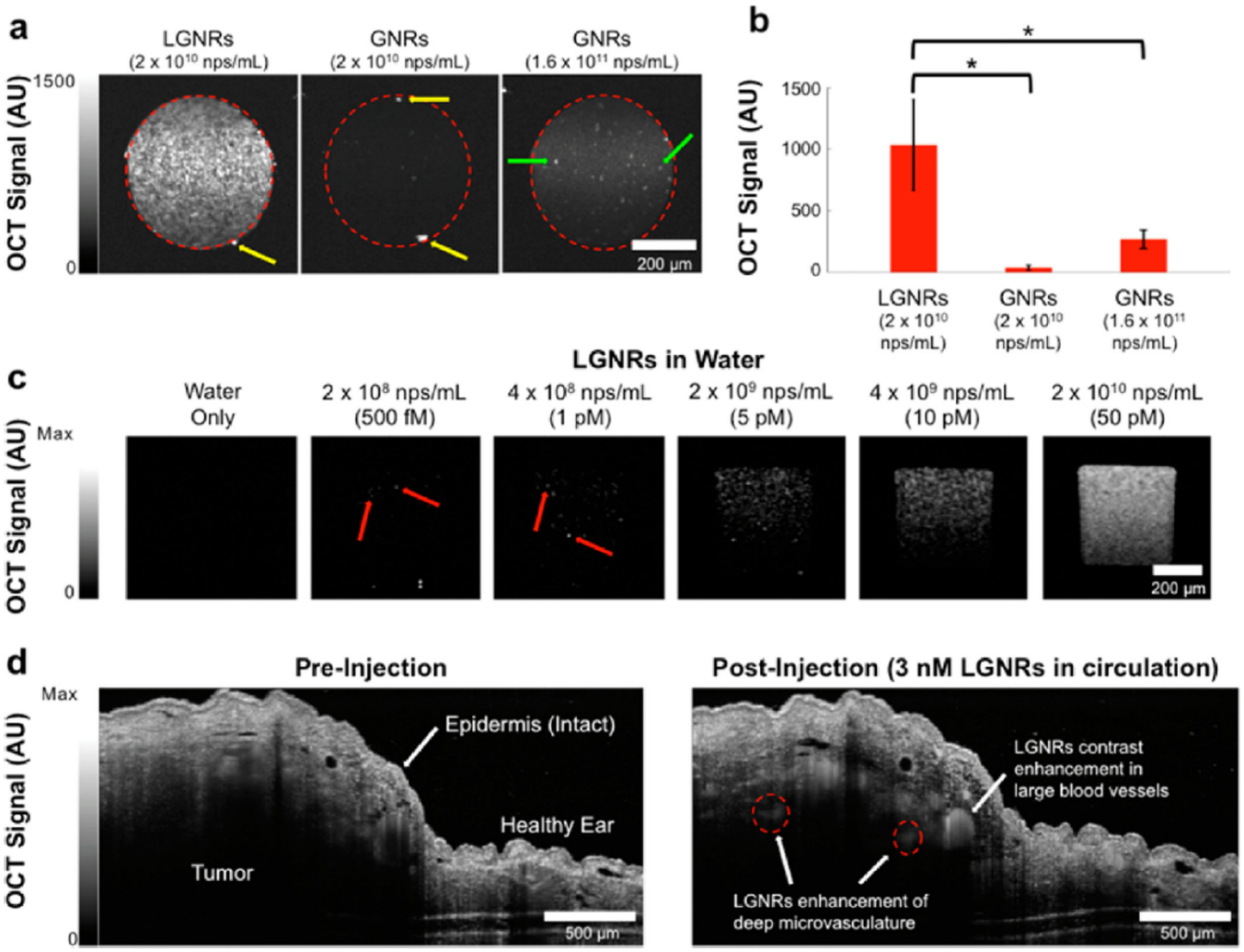

Figure 5.

LGNRs are highly effective OCT contrast agents that enable single particle sensitivity in vitro and nanomolar sensitivity for noninvasive in vivo imaging. (a) Linear-scale OCT B-scans of LGNRs and two concentrations of GNRs show that LGNRs scatter significantly more near-infrared light (~800 nm) than GNRs of equivalent plasmonic resonance per nanoparticle. LGNRs also display stronger scattering than GNRs even when LGNRs and GNRs are prepared to equal mass concentration (2×10^{10} nps/mL for LGNRs and 1.6×10^{11} nps/mL for GNRs; the 8-fold increased GNR concentration accounts for the particle volume difference between LGNRs and GNRs). (b) Region of interest analysis shows that LGNRs exhibit ~4-fold greater scattering than GNRs prepared to equivalent mass concentration. Considering the 4-fold greater LGNRs signal as well as the 8-fold difference in particle concentrations, LGNRs can produce up to ~32-fold greater OCT contrast than GNRs per particle (*$p < 0.0001$). Yellow arrows indicate specular reflections from capillary tubes. Green arrows show examples of spherical impurities ($d \sim 50$ nm) present in GNR solutions. (c) LGNRs produce enough scattering to enable detection of individual LGNRs in water. When prepared to 500 fM, the number of LGNRs expected to be present within the imaged capillary volume is ~70. This number is roughly consistent with the number of discrete

puncta observed in the sample tube. The total signal increases for higher LGNR concentrations. Red arrows point to selected single LGNRs. (d) LGNRs-PSS-mPEG (250 μL of 23.5 nM) were tail vein-injected into a nude mouse bearing a U87MG tumor xenograft in the right ear pinna to achieve a particle concentration of 3 nM in circulation. OCT B-scans were acquired (completely noninvasively) before and after injection. LGNR-PSS-mPEG contrast results in increased OCT signal in blood vessels. LGNR-PSS-mPEG contrast-enhancement reveals small blood vessels (red dashed circles) deep within the tumor that cannot be visualized prior to injection.